

## Wind and Turbulence in a Sparse but Regular Plant Canopy

ANDREE TUZET

*Institut National de la Recherche Agronomique, Paris, France*

JOHN D. WILSON

*Department of Earth and Atmospheric Sciences, University of Alberta, Edmonton, Canada*

(Manuscript received 27 December 2000, in final form 30 October 2001)

### ABSTRACT

Wind velocity statistics from several points within a regular but sparse array of clumped corn plants are analyzed, with each clump consisting of 12 plants, having a mean height of 1.6 m and a collective leaf area of about 2.75 m<sup>2</sup> and occupying approximately 0.8 m<sup>2</sup> of ground area. The clumps defined the (484) nodes of a square lattice, with side length of 5.6 m, and this lattice covered an area of 120 m × 120 m within an otherwise uniform corn field. Forty-eight half-hour records of daytime mean “cup” wind speeds and turbulent kinetic energies  $k$ , from several points in the canopy, are displayed against a “reduced” mean wind direction that exploits the symmetries of the canopy. These data conform well with the corresponding fields from a three-dimensional, steady-state wind model (with eddy viscosity  $\propto \lambda k^{1/2}$ , where  $\lambda$  is the length scale). Both the observations and the model confirm the importance of a set of special wind directions, some of which place a given point P in the shelter of a nearby clump (“blockage”) and others of which place P in a “corridor.”

### 1. Introduction

Sparse and/or irregular plant canopies occupy much of the global land surface, and their interaction with the wind generates highly disturbed, locally inhomogeneous flow. In these circumstances, Monin–Obukhov surface layer similarity theory is inapplicable, and we lack a framework for the analysis of wind-mediated processes such as spray, seed, and pollen dispersal; of soil evaporation; and so forth. There is an infinity of particular cases of disturbed winds that are unified only in the sense that all are governed by the conservation equations (momentum, mass, and energy). Therefore it is important that wind models for flows over an inhomogeneous surface be tested to establish their competence. As an example, suppose one wished to estimate the spatial average subcanopy evaporation rate  $\langle E \rangle$  under a sparse canopy: even supposing a uniformly bare and saturated soil, the local evaporation rate  $E = E(x, y)$ , where  $x$  and  $y$  are horizontal directions, varies according to the local wind, temperature, and humidity, and so a micrometeorological model, used as an interpolative tool in conjunction with a set of measured inputs, is a rational approach. An equally compelling challenge for wind models would be to provide the wind

statistics needed to infer the spread of pollen from widely scattered shrubs.

Measurements in a sparse, random canopy present a daunting challenge, namely, how to provide a complete yet economical representation of the flow statistics from measurements taken at only a few points. To sidestep this problem, we created an unusual and artificial sparse canopy that has perfect geometrical regularity (Fig. 1). We compare wind measurements made within this idealized canopy with a three-dimensional, steady-state wind model, focusing especially on the variation of wind statistics versus the wind *direction* relative to the axes of the array, an angle we call the “reduced” wind direction  $\beta$  because, at each of the observation points chosen, angular symmetries of the array render certain distinct (absolute) wind directions  $\theta$  to be *equivalent*.

### 2. Experiment

#### a. Sparse canopy

The experiment took place at the Institut National de la Recherche Agronomique (INRA) research station at Grignon (Paris) during August of 1997. The sparse canopy (Figs. 1 and 2) constituted a square lattice, based on a unit cell of side length  $d = 5.6$  m, and covered an area of 120 × 120 m<sup>2</sup>. This lattice (our sparse canopy) was enclosed within a uniform field of corn [canopy height  $h_{\text{env}} = 2$  m, leaf area index (LAI) = 3] that

*Corresponding author address:* Andree Tuzet, Institut National de la Recherche Agronomique, E.G.C., 78850 Thiverval-Grignon, France.  
E-mail: tuzet@bcgn.grignon.inra.fr



FIG. 1. Photograph of sparse canopy of clumps of maize, at the INRA research station near Grignon, France. Spacing of the clumps is  $d = 5.6$  m. Note the visible axes of symmetry.

extended at least 100 m in every direction from the boundary of sparse canopy.

At the vertices of the array were “clumps” of (on average) 12 corn plants, arranged in hexagons of (approximately) 1 m in diameter. At the time of the experiment, the clumps had an average height  $h$  of approximately 1.6 m, occupied about  $0.8 \text{ m}^2$  of ground area, and had a total (per clump) leaf area of approximately  $2.8 \text{ m}^2$ . Outside the “drag nodes” (i.e., the clumps), the sparse canopy consisted of empty space, but for a low cover of weeds ( $h_w = 0.2$  m).

The topography of the site, although not perfectly level, should not have caused a disturbance to the wind nearly as significant as that of encountering the (mostly) open space of our array, in which only “pulses” of canopy drag occurred, at the widely separated clumps. The sparsity of the canopy is visually evident in Fig. 1 and is indicated by the low overall LAI [ $= (484 \times 2.8 \text{ m}^2) / 120^2 = 0.09$ ]; whereas, in contrast, the LAI of the weed cover was measured to be  $\text{LAI}_{\text{weed}} = 2.5$ ].

#### b. Defining the background flow

A 20-m tower within the array supported cup anemometers (Cimel Electronique, Inc.) and shielded, ventilated thermocouples ( $z/h = 0.34, 0.64, 0.97, 1.46, 2.21, 3.34, 4.40, 5.05, 6.20, 7.62, 9.32, \text{ and } 11.52$  m), providing the mean wind and temperature profiles  $\bar{u}(z)$  and  $\bar{T}(z)$  above the canopy. A wind vane on the tower [Campbell Scientific, Inc. (CSI)] recorded the (true) mean wind direction  $\theta$  (measured w.r.t. magnetic north). From these

data, we derived for each experimental interval the surface layer scaling parameters  $u_{*p}$  (friction velocity from profiles),  $L$  (Obukhov length), and  $\theta_*$  (turbulent temperature scale); these parameters are defined by

$$u_*^2 = \left[ \frac{k_v(z - z_d)u_*}{\phi_m(z)} \right] \frac{\Delta \bar{u}}{\Delta z},$$

$$u_* \theta_* = \left[ \frac{k_v(z - z_d)u_*}{\phi_h(z)} \right] \frac{\Delta \bar{\theta}}{\Delta z}, \quad \text{and}$$

$$L = \frac{u_*^2}{k_v(g/T_0)\theta_*}, \quad (1)$$

where  $z_d$  is the displacement length,  $k_v$  is the von Kármán constant,  $g/T_0$  is the buoyancy parameter, and  $\phi_m$  and  $\phi_h$  the universal functions. For  $\phi_m$  and  $\phi_h$ , under the unstable conditions encountered, we assumed the formulas (Dyer 1974)

$$\phi_m(z) = \left( 1 + 16 \left| \frac{z}{L} \right| \right)^{-1/4}, \quad \text{and}$$

$$\phi_h(z) = \left( 1 + 16 \left| \frac{z}{L} \right| \right)^{-1/2}. \quad (2)$$

The method used to calculate the scaling parameters ( $u_*$ ,  $\theta_*$ , and  $L$ ) consists of the simultaneous solution of (1) and (2) with known measurements of wind speed differences and temperature differences between pairs of

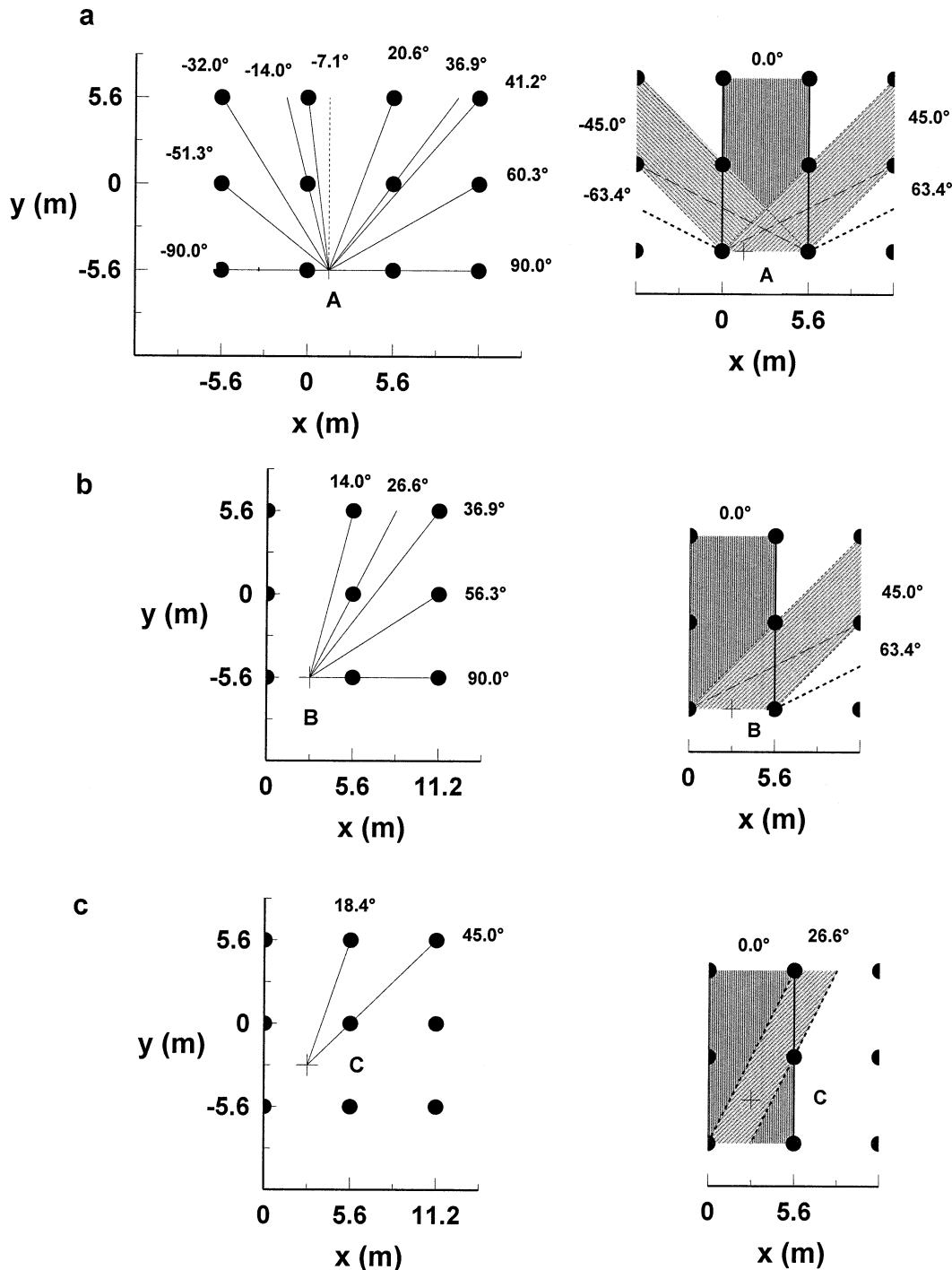


FIG. 2. Frame of reference for the sparse canopy, and identification of measurement locations (A, B, C) and the most important blockage and corridor angles  $\beta$ : (a) blockage and corridor angles for the A location (distance  $d/4$  from clump, along any side), with reduced wind direction  $\beta$  defined such that  $\beta$  is equal to  $-90^\circ$  for a wind blowing from left to right along the  $x$  axis; (b) blockage and corridor angles for the B location (distance  $d/2$  from clump, along any side)—owing to the higher degree of symmetry, the domain for reduced wind direction is  $0^\circ \leq \beta \leq 90^\circ$ , with corridors at  $\beta = 0^\circ, 45^\circ$ , and  $63.4^\circ$ ; (c) blockage and corridor angles for the C location [midpoint  $(x, y) = (\pm 1/2d, \pm 1/2d)$  of a unit cell]—owing to the higher degree of symmetry, the domain for reduced wind direction is  $0^\circ \leq \beta \leq 45^\circ$ , with corridors at  $\beta = 0^\circ$  and  $26.6^\circ$ .

TABLE 1. Details of each 30-min run of the Grignon sparse-canopy experiments (local time,  $u_{*p}$  is the friction velocity from profiles,  $L$  is the Obukhov length,  $\theta_*$  is the turbulent temperature scale, and  $\bar{\theta}$  is the mean wind direction).

| Day | Time ending | $u_*$ (m s <sup>-1</sup> ) | $\theta_*$ (K) | $L$ (m) | $\bar{\theta}$ |
|-----|-------------|----------------------------|----------------|---------|----------------|
| 3   | 1240        | 0.366                      | -0.714         | -14.40  | -162.98        |
| 3   | 1310        | 0.356                      | -0.714         | -13.61  | -172.1         |
| 3   | 1340        | 0.366                      | -0.687         | -14.65  | -170.81        |
| 3   | 1500        | 0.375                      | -0.539         | -19.56  | 170.64         |
| 3   | 1530        | 0.366                      | -0.425         | -23.79  | 177.57         |
| 3   | 1600        | 0.355                      | -0.341         | -28.61  | -176.96        |
| 3   | 1705        | 0.345                      | -0.333         | -29.44  | 165.29         |
| 3   | 1735        | 0.334                      | -0.106         | -84.41  | 171.78         |
| 3   | 1805        | 0.337                      |                |         | 157.17         |
| 4   | 1400        | 0.279                      | -0.742         | -7.74   | -50.779        |
| 4   | 1430        | 0.276                      | -0.445         | -12.99  | -58.125        |
| 4   | 1500        | 0.284                      |                |         | -63.718        |
| 5   | 1300        | 0.172                      | -0.742         | -3.23   | 4.4312         |
| 5   | 1330        | 0.218                      | -0.611         | -6.00   | -31.754        |
| 5   | 1400        | 0.269                      | -0.614         | -8.87   | -48.275        |
| 5   | 1445        | 0.268                      | -0.376         | -14.71  | -55.315        |
| 5   | 1515        | 0.281                      | -0.358         | -16.88  | -60.722        |
| 5   | 1545        | 0.275                      | -0.405         | -14.00  | -48.968        |
| 8   | 1430        | 0.314                      | -0.580         | -12.67  | -34.765        |
| 8   | 1500        | 0.277                      | -0.770         | -7.67   | -36.933        |
| 8   | 1530        | 0.276                      | -0.900         | -6.26   | -69.165        |
| 8   | 1635        | 0.235                      | -0.786         | -5.32   | -80.381        |
| 8   | 1705        | 0.263                      | -0.535         | -9.68   | -92.747        |
| 8   | 1735        | 0.285                      | -0.391         | -16.16  | -61.576        |
| 9   | 1420        | 0.296                      | -0.526         | -12.47  | -22.391        |
| 9   | 1450        | 0.336                      | -0.444         | -19.09  | -28.983        |
| 9   | 1520        | 0.336                      | -0.618         | -13.77  | -2.0314        |
| 9   | 1635        | 0.372                      | -0.515         | -20.44  | -16.644        |
| 9   | 1705        | 0.322                      | -0.418         | -19.66  | -16.99         |
| 9   | 1735        | 0.373                      | -0.334         | -33.46  | -17.838        |
| 10  | 1230        | 0.506                      | -0.522         | -37.09  | 70.973         |
| 10  | 1300        | 0.489                      | -0.570         | -31.18  | 62.969         |
| 10  | 1330        | 0.462                      | -0.659         | -24.94  | 66.784         |
| 10  | 1430        | 0.409                      | -0.645         | -19.66  | 68.415         |
| 10  | 1500        | 0.424                      | -0.574         | -24.08  | 64.467         |
| 10  | 1530        | 0.421                      | -0.504         | -26.54  | 62.437         |
| 10  | 1625        | 0.449                      | -0.414         | -38.18  | 50.984         |
| 10  | 1655        | 0.420                      | -0.352         | -41.04  | 50.479         |
| 10  | 1725        | 0.398                      | -0.277         | -49.21  | 45.743         |
| 11  | 1200        | 0.303                      | -0.651         | -10.83  | 159.14         |
| 11  | 1230        | 0.373                      | -0.707         | -14.93  | -166.7         |
| 11  | 1300        | 0.388                      | -0.672         | -16.78  | -175.99        |
| 11  | 1410        | 0.407                      | -0.599         | -20.82  | 170.71         |
| 11  | 1440        | 0.403                      | -0.544         | -22.51  | 166.65         |
| 11  | 1510        | 0.422                      | -0.455         | -29.53  | 170.06         |
| 11  | 1620        | 0.430                      | -0.252         | -57.71  | 179.66         |
| 11  | 1650        | 0.408                      | -0.188         | -72.72  | -162.83        |
| 11  | 1720        | 0.415                      | -0.134         | -108.76 | -156.75        |

heights above the canopy. Table 1 lists the scaling parameters for all runs.

### c. Placement of fast-response anemometers in the sparse canopy

Four 3D sonic anemometers [two Gill Instruments, Ltd., R2 and two CSI CSAT-3] were available to sample the disturbed turbulent flow. To investigate the consistency of the Gill and CSI anemometers, we ran a CSAT-3 beside the reference Gill ( $S_{ref}$ ) for three 30-min intervals. The 30-min mean cup wind speeds from the two instruments differed by less than 10 cm s<sup>-1</sup>, representing

an uncertainty in that property of about 5%. Corresponding differences in component standard deviations  $\sigma_u$ ,  $\sigma_v$ , and  $\sigma_w$  were less than 3 cm s<sup>-1</sup>, or about 4%. Thus the Gill and CSI sonic anemometers proved adequately consistent for our purposes.

One Gill sonic anemometer ( $S_{ref}$ ) was placed well above the canopy, at a reference level  $z_{ref} = 3.2$  m ( $z_{ref}/h = 2$ ), to provide a normalizing (reference) velocity scale (the friction velocity  $u_{*r}$  or the standard deviation of vertical velocity  $\sigma_{wr}$ ); nevertheless, on some figures a friction velocity  $u_{*p}$  derived from the mean wind and temperature profiles has been used as the normalizing scale. We assumed the reference level to be high enough

TABLE 2. The most important symmetry angles ( $^{\circ}$ ) for locations A, B, and C in the regular sparse canopy of Figs. 1 and 2. "Fetch" is the distance (in multiples of  $d$ ;  $=5.6$  m) to the nearest clump, along the given direction  $\beta$  from the point of observation (A, B, or C); "width" is the distance (in multiples of  $d$ ) between pairs of boundary lines along direction  $\beta$ , which define a corridor relative to A, B, or C.

| A         |       |           |       | B         |       |           |       | C         |       |           |       |
|-----------|-------|-----------|-------|-----------|-------|-----------|-------|-----------|-------|-----------|-------|
| Blockages |       | Corridors |       | Blockages |       | Corridors |       | Blockages |       | Corridors |       |
| $\beta$   | Fetch | $\beta$   | Fetch | $\beta$   | Fetch | $\beta$   | Width | $\beta$   | Fetch | $\beta$   | Width |
| -90.0     | 0.25  | -63.4     | 0.45  | +14.0     | 2.06  | 0.0       | 1.0   | +18.4     | 1.58  | 0.0       | 1.0   |
| -51.3     | 1.60  | -45.0     | 0.71  | +26.6     | 1.12  | +45.0     | 0.71  | +45.0     | 0.71  | +26.6     | 0.45  |
| -32.0     | 2.36  | 0.0       | 1.0   | +36.9     | 2.50  | +63.4     | 0.45  |           |       |           |       |
| -14.0     | 1.03  | +45.0     | 0.71  | +56.3     | 1.80  |           |       |           |       |           |       |
| -7.1      | 2.02  | +63.4     | 0.45  | +90.0     | 0.50  |           |       |           |       |           |       |
| +20.6     | 2.14  |           |       |           |       |           |       |           |       |           |       |
| +36.9     | 1.25  |           |       |           |       |           |       |           |       |           |       |
| +41.2     | 2.66  |           |       |           |       |           |       |           |       |           |       |
| +60.3     | 2.02  |           |       |           |       |           |       |           |       |           |       |
| +90.0     | 0.75  |           |       |           |       |           |       |           |       |           |       |

that flow statistics at that level should be roughly constant in the horizontal plane over distances on the order of the unit length  $d$  and, more important, should not vary in response to changes in mean wind direction  $\bar{\theta}$ . Only by virtue of the latter assumption can we justify using  $\sigma_{wr}$  (or  $u_{*r}$ ) to normalize measured velocity statistics from the other three instruments ( $S_0$ ,  $S_1$ , and  $S_2$ ), statistics assembled from differing locations and time intervals, to "map" the (by hypothesis, approximately invariant) spatial pattern of the flow in the sparse canopy.

The other three sonic anemometers ( $S_0$ ,  $S_1$ , and  $S_2$ ) were used to probe the in-canopy details of the flow. We need make reference only to the coordinates  $(x, y)$  of a measurement location, *relative* to (any) corner node supplemented by specification of the (reduced) mean wind direction  $\bar{\beta}$ , defined relative to (any) axis of the array. We always placed the second Gill anemometer ( $S_0$ ) at the midpoint  $(x, y) = (\pm 1, \pm 1)d/2$  of a unit cell (location "C"), most often at  $z/h = 0.75$ . The other (CSI) sonic anemometers were each placed at  $z/h = (0.5, 0.75, \text{ or } 1)$ , on one or another of the sides of (any) unit cell, that is, at locations restricted to  $(x, y) = (n_x, n_y)d/4$ , where  $n_x, n_y = (0, 1, 2, 3)$ ; instruments were never placed at  $n_x = n_y = 0$ , i.e., within a clump). These placements imply that the locations of ( $S_1, S_2$ ) in the  $x$ - $y$  plane, relative to a unit cell, took on only two values, labeled (A, B). Figure 2 shows the three sonic anemometer locations (A, B, C) in a unit cell.

Prior to each run, the CSI sonic anemometers ( $S_1, S_2$ ) were oriented by eye, with an uncertainty of, at worst, about  $\pm 5^{\circ}$ , so as to face either normal or parallel to the side of a cell. This adjustment ensured that the wind fell predominantly within the frontal approach angle of the instrument (longitudinal velocity component relative to the instrument frame,  $u_r > 0$ ). Subsequent analysis indicated that for most runs, flow "reversals" were infrequent.

#### d. Data acquisition and coordinate rotations

Simultaneous digital wind speed signals from the two CSI anemometers were measured and recorded by a

single CSI CR10X datalogger, at a sampling frequency  $f = 16$  Hz, and were written to a Personal Computer Memory Card International Association (PCMCIA) card. After each 90-min run, the PCMCIA card was inserted in a laptop computer, and the data were transferred to a hard disk. The signals from each of the two Gill instruments were recorded throughout the same 90-min intervals, on two different dataloggers (CSI CR23X), at a sampling frequency of 20.83 Hz (i.e., Gill signals were not synchronous with each other nor with the CSI signals). For the analysis of these data, we subdivided the 90-min records into 30-min runs. We gathered a total of 24 h of noncontinuous daytime measurements, all of which are represented in the results to follow; we performed no filtering of these data.

Orientations of the Gill anemometers on their respective towers were difficult to control precisely, and so those time series were subjected to a coordinate rotation that rendered the 30-min mean vertical velocity  $\bar{w}$  equal to 0. The necessity to take that step is unfortunate (in reality,  $\bar{w}$  need not vanish in our disturbed flow). The CSI sonic anemometers were believed to be level to within about  $\pm 1^{\circ}$ , and therefore no rotations were performed.

For each 30-min run, mean wind direction  $\bar{\theta}$  is cited relative to the north magnetic axis, which corresponded closely to a symmetry axis of the array (Fig. 2). This particular wind direction is of no special significance, however, and, for *each* run and *each* anemometer, a local mean wind direction, relative to the frame of the instrument, was calculated (from the raw time series of  $u$  and  $v$ ) as  $\bar{\beta}_f = \tan^{-1}(\bar{v}/\bar{u})$ . To calculate certain statistics, it was necessary to determine time series of velocities relative to this local mean wind direction; that is,

$$\begin{aligned} u_r &= u \cos \bar{\beta}_f + v \sin \bar{\beta}_f \quad \text{and} \\ u_r &= -u \sin \bar{\beta}_f + v \cos \bar{\beta}_f. \end{aligned} \quad (3)$$

Velocity statistics cited in this "locally reoriented" coordinate system are the standard deviation  $\sigma_{\beta}$  of the wind direction (this was done so as to avoid errors aris-

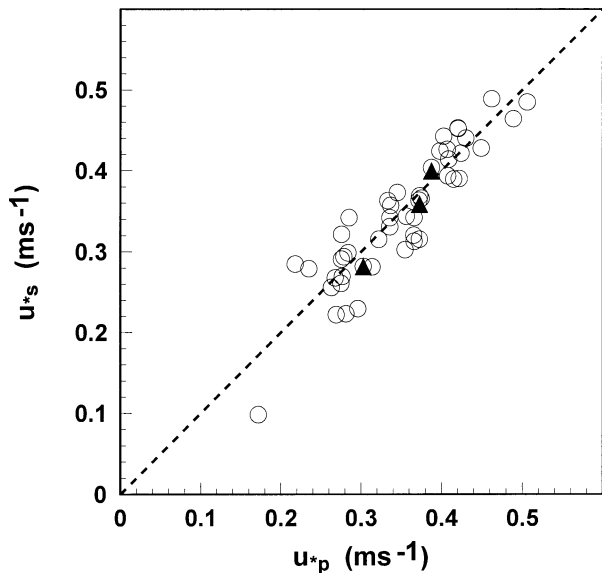


FIG. 3. Comparison of friction velocity  $u_{*p}$  derived from tower profiles with that derived from the shearing stress ( $u_* = \sqrt{-u'w'}$ ) measured by the reference sonic anemometer ( $\circ$ ) at  $z/h = 2$  (after a rotation set  $\bar{v} = \bar{w} = 0$ ) and (for three intervals only) with that measured by a CSI sonic anemometer ( $\blacktriangle$ ) placed beside the reference sonic anemometer.

ing from the periodicity of the circular functions) and the standard deviations  $\sigma_u$  and  $\sigma_v$  of the alongwind and lateral components (because it is usual to reserve the symbol  $\sigma_u$  for an alongwind component).

*e. Implications of symmetries for interpretation of the wind statistics*

In each location, wind statistics vary as a function of the mean wind direction  $\theta$  as recorded on the tower. Due to the symmetry of the array, however, at A the domain of dependence of flow statistics covers (theoretically) only a smaller range,  $-90^\circ \leq \bar{\beta} \leq 90^\circ$ , in the reduced wind direction  $\bar{\beta}$ ; at B the reduced range is only  $0^\circ \leq \bar{\beta} \leq 90^\circ$ , and at C the domain is restricted even further to  $0^\circ \leq \bar{\beta} \leq 45^\circ$ . Thus, in a relatively small number of experimental runs, by exploiting variation of absolute mean wind direction, we hoped to establish the functional dependence of wind statistics on the full domain for the reduced wind direction.

The wind could approach any measurement point from special angles corresponding to “corridors” (no clumps upwind) and “blockages” (a clump lying upwind, at some lesser or greater range). In principle, there exists an infinite number of these special approach angles, but we concentrated on the most important, which are listed in Table 2. Some features of the results to follow can be understood in terms of these special angles.

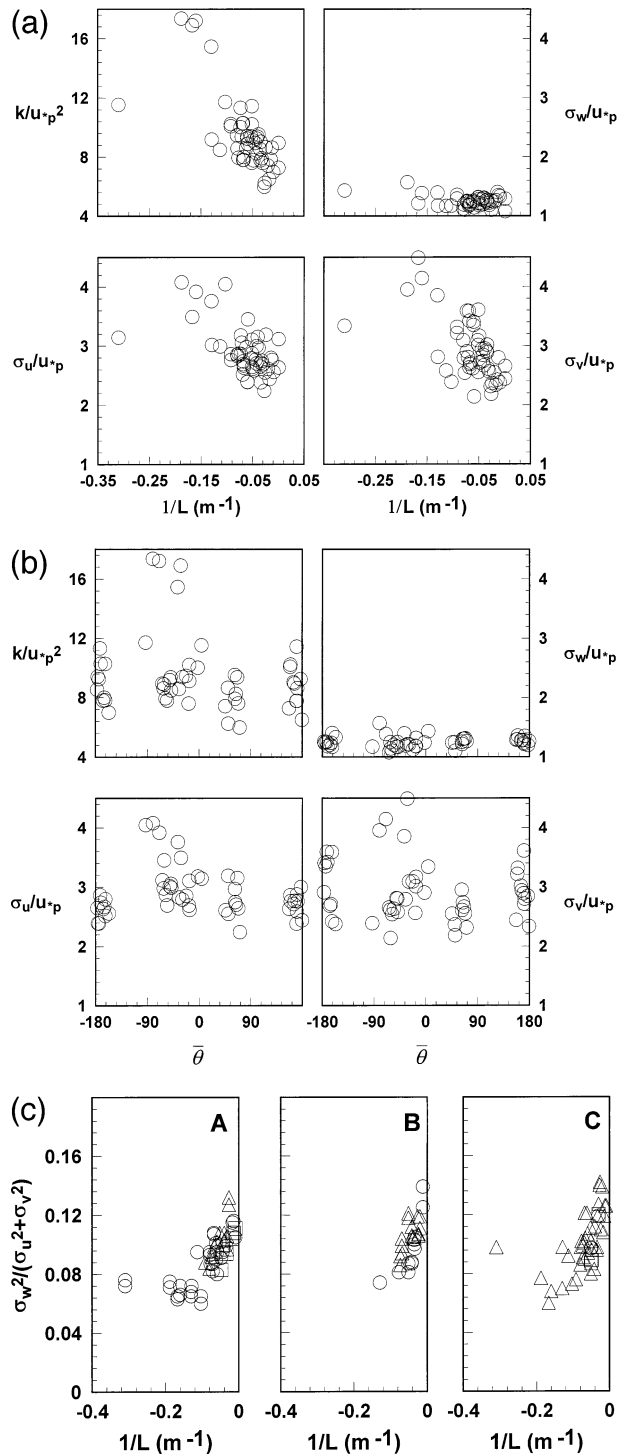


FIG. 4. Normalized standard deviations  $\sigma_u/u_{*p}$ ,  $\sigma_v/u_{*p}$ , and  $\sigma_w/u_{*p}$  and TKE  $k/u_{*p}^2$ , measured by the reference sonic anemometer at  $z/h = 2$  (after a rotation set  $\bar{v} = \bar{w} = 0$ ), vs (a)  $1/L$  and (b) wind direction  $\theta$ . (c) Observations of the ratio  $\sigma_w^2/(\sigma_u^2 + \sigma_v^2)$  at all points (A, B, C) within the canopy, at heights  $z/h = 1/2$  ( $\circ$ ),  $3/4$  ( $\triangle$ ), and  $1$  ( $\square$ ) vs  $1/L$ . The equilibrium value inferred from the reference sonic anemometer at  $z/h = 2$  is about 0.093.

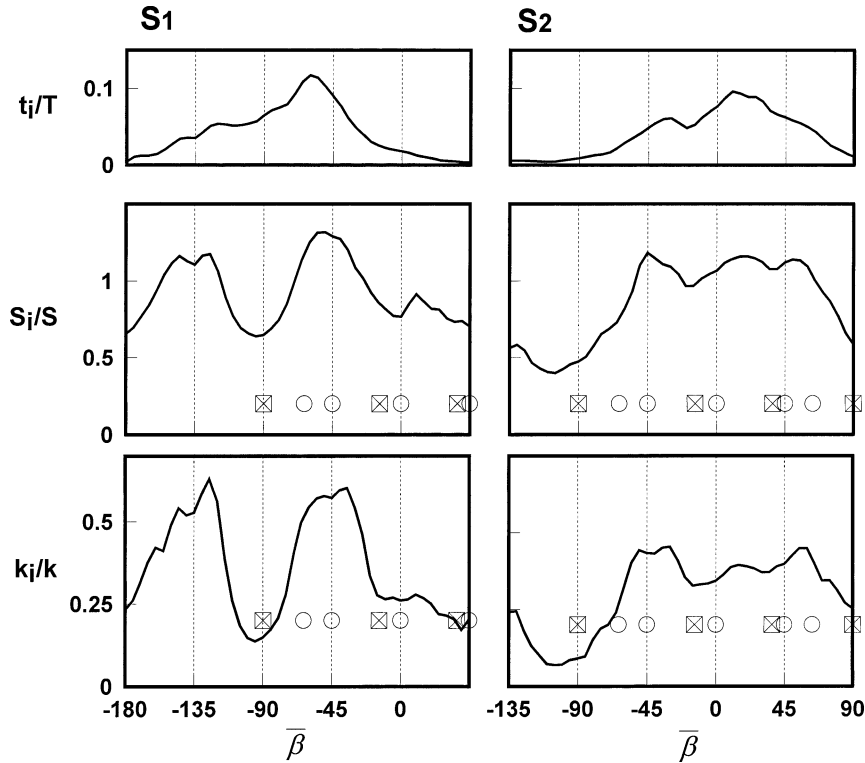


FIG. 5. Simultaneous histograms for wind direction (time fraction  $t_i/T$  within each  $5^\circ$  wind direction bin  $i$ ) at sonic anemometers ( $S_1$ ,  $S_2$ ), both at A locations (but oriented differently with respect to the mean wind  $\bar{\theta}$  relative to north), and respective conditional mean values within bins for cup wind speed  $S$  and TKE  $k$ , normalized on the respective unconditional means. Also indicated are important blockage angles ( $\square$ ) and corridor angles ( $\circ$ ) for A locations. On the horizontal axis, wind direction  $\beta = 0^\circ$  is the zero of the scale for reduced wind direction, but (here) observations were *not* folded into the (theoretically, entire) domain  $-90^\circ \leq \beta \leq 90^\circ$  in order that the expected symmetries may be sought. Data are from 1300–1329 local time 5 Sep.

### 3. Numerical model

#### a. Governing equations

The wind model used in this study is a generalization to three dimensions of that described by Wilson et al. (1998) and Wilson and Flesch (1999). Because it already has been documented well, we shall review only briefly its form and specify modifications relative to the earlier work.

Spatially varying momentum sinks are introduced into the steady-state mean momentum equations; for example, because of the air–vegetation interaction, the streamwise ( $\bar{u}$ ) momentum equation is

$$\frac{\partial}{\partial x} \left( \bar{u}^2 + \overline{u'^2} + \frac{\bar{p}}{\rho} \right) + \frac{\partial}{\partial y} (\bar{u} \bar{v} + \overline{u'v'}) + \frac{\partial}{\partial z} (\bar{u} \bar{w} + \overline{u'w'}) = -c_d a \bar{u} U, \quad (4)$$

where the terms have their usual meaning; velocities are decomposed into the sum of a mean and fluctuation,  $u_i = \bar{u}_i + u'_i$ , so that, for example,  $\overline{u'^2}$  is the variance of the fluctuation in horizontal velocity about the mean

$\bar{u}$ . Equation (4) is valid under the Boussinesq approximation, and  $\bar{p}$  is the mean pressure *departure* from an adiabatic, hydrostatic reference state. Our model *neglects* any influence of atmospheric stratification. The right-hand side of (4) is the projection onto the  $x$  axis of a drag force, proportional to the square of the local mean velocity  $U = \sqrt{\bar{u}^2 + \bar{v}^2 + \bar{w}^2}$ . The plant area density  $a = a(x, y, z)$  vanishes above the weed cover (i.e., for  $z > z_w$ ), except within the clumps of maize, where it was specified as constant on the basis of the measured leaf area of the clumps, which implied a leaf area  $A$  of about  $2.2 \text{ m}^{-1}$ . The drag coefficient  $c_d$  of the vegetation could not be determined from the available data, and so we treated the dimensionless group  $c_d Ah$  as a free parameter, the sole such parameter in the model.

A minor modification relative to earlier simulations with this model is that components of the Reynolds stress tensor that previously had been neglected (being replaced, in effect, by small “artificial” diffusion terms) were specified conventionally; that is, the stress tensor was parameterized as

$$\overline{u'_i u'_j} = \alpha_{ij} k - K \left( \frac{\partial \bar{u}_i}{\partial x_j} + \frac{\partial \bar{u}_j}{\partial x_i} \right), \quad (5)$$

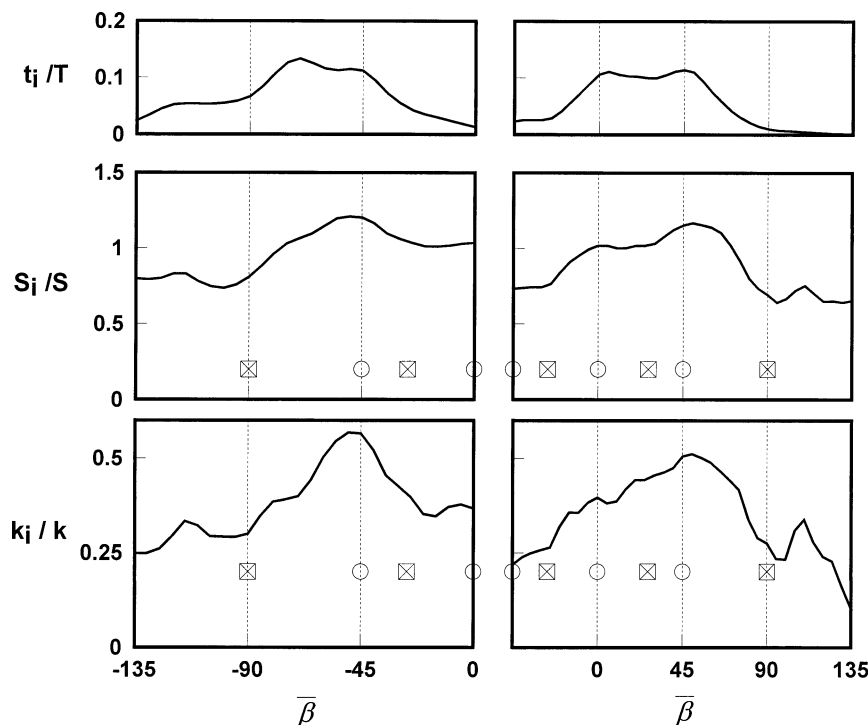


FIG. 6. As in Fig. 5, but for instruments at B locations (1240–1309 local time 3 Sep). In principle, the domain  $0^\circ \leq \beta \leq 90^\circ$  is entire; that is, statistics ( $S_j/S$ ,  $k_j/k$ ) outside this quadrant ought to be equivalent because of reflection symmetry.

where  $\alpha_{ij}$  is diagonal, and gives the reference (or equilibrium) values for the ratios of the velocity variances to the turbulent kinetic energy (TKE)  $k$ , for example,  $\alpha_{11} = \overline{u'^2}/k$ , (etc.). The eddy viscosity  $K$  was parameterized as earlier by  $K = \lambda \sqrt{c_e} k$ , where  $c_e$  is simply the equilibrium value of the ratio  $u_{*p}^2/k$  and  $\lambda$  is an imposed length scale.

The success of such a simple closure hinges on specification of the length scale, and we followed the earlier pattern with this closure, namely,  $\lambda = \max(\lambda_i, \lambda_o)$ . For large values of  $z$  (“outer region”), the length scale is given by

$$\frac{1}{\lambda_o} = \frac{1}{k_v(z - z_d)}, \quad (6)$$

where  $k_v$  is the von Kármán constant. The displacement length  $z_d$  was (in this study) treated as spatially invariant, and, because of the low value of the overall clump leaf area index (LAI = 0.09), it was considered to be determined by the weed cover: we set  $z_d = 0.75h_w$ .

For small values of  $z$  (“inner region”), the length scale is given by

$$\frac{1}{\lambda_i} = \frac{1}{k_v z} + \frac{1}{\lambda_h} \quad (7)$$

and so cannot exceed the canopy-shear length scale (Raupach et al. 1996),

$$\lambda_{hc} = \frac{ck_{hc}^{1/2}}{\left[ \left( \frac{\partial \bar{u}}{\partial z} \right)^2 + \left( \frac{\partial \bar{v}}{\partial z} \right)^2 \right]^{1/2}}. \quad (8)$$

In broad terms, the numerical model functions as follows: (4) expresses conservation of  $\bar{u}$  momentum at each and every point. The job of the numerical procedure, which uses a finite-difference approximation to (4) and the other equations, is to calculate the *unique* gridded spatial fields of mean wind and TKE that are consistent with the differential equations (i.e., that respect mass and momentum conservation locally), with the chosen boundary conditions (e.g., the constant shear stress  $\overline{u'w'}$  at the top of the domain implies a downward flow of  $\bar{u}$  momentum across the top boundary), and with the internal sinks [notably the canopy drag term in (4)]. Under the (assumed) condition of lateral periodicity of the wind (infinite repetition of unit cells of the plant array), the key inputs are the distribution of plants and the plant drag coefficient within a unit cell (the  $c_d A$  product) and the upper boundary momentum flux (given by  $-u_{*p}^2$ , but note that if the imposed stress is set to  $-1$ , the model calculates velocity statistics that are normalized on  $u_{*p}$ ).

#### b. Computational details

Neglecting the inevitable departures from symmetry of our array, we can regard the sparse canopy (Figs. 1

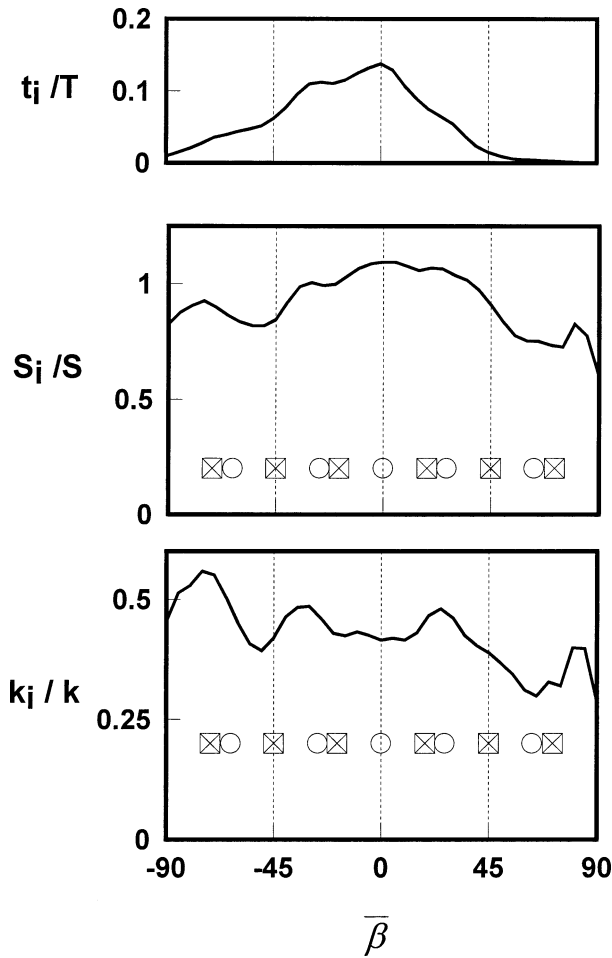


FIG. 7. As in Figs. 5 and 6, but for an instrument at C ( $z/h = 0.5$ ; 1635–1704 local time 9 Sep).

and 2) as being characterized by the repetition of an identical unit cell. Then the (mean) velocity field ideally must repeat itself, cell by cell. It therefore is possible to impose periodic boundary conditions (period  $d = 5.6$  m), and so the model domain covered only a single unit cell of our sparse canopy. The upper boundary of the computational domain was set at  $z = 4h$ . In simulations shown, the horizontal dimensions of control volumes were constant,  $\Delta x = \Delta y = 0.2$  m ( $=d/28$ ); vertical resolution was  $\Delta z/h = 0.125$  for  $z/h \leq 1$  and increased logarithmically in the range  $1 \leq z/h \leq 4$ .

The observations did not determine the value of the bulk drag coefficient  $c_d Ah$  of the clumps of maize, although the known leaf area density establishes that  $Ah$  is equal to 3.5. Model results to follow correspond to the specification  $c_d Ah = 0.5$ . Because of the use of a staggered grid, control volumes falling across edges of clumps of maize were filled only partially, and the bulk drag parameter  $c_d Ah$  for such cells was reduced accordingly.

The flow was driven by imposed (constant) shear stresses  $\overline{u'w'}$ ,  $\overline{v'w'}$  along  $z/h = 4$ , and these stresses

were adjusted to ensure any desired mean wind direction  $\bar{\theta}$  aloft:

$$\begin{aligned} \overline{u'w'}(4h) &= -u_{*0}^2 \cos(\bar{\theta}), \quad \text{and} \\ \overline{v'w'}(4h) &= -u_{*0}^2 \sin(\bar{\theta}), \end{aligned} \quad (9)$$

with  $u_{*0}^2 = 1$ . There was no background pressure gradient, though, of course, the interaction of the wind with the vegetation generated a disturbed pressure field. Iterations were continued until imbalances in the globally integrated (i.e., whole domain)  $\bar{u}$ - and  $\bar{v}$ -momentum equations were reduced below 2% of the respective totals of the drag on the enclosed vegetation.

Turbulent velocity standard deviations measured at  $z/h = 2$ , above the sparse canopy, were about  $\sigma_u/u_* = \sigma_v/u_* = 3$  and  $\sigma_w/u_* = 1.3$  except during runs of the most unstable stratification (see Fig. 4, described below). Thus, in simulations we set the reference values  $c_e = u_*^2/k = 0.102$ ,  $\alpha_{11} = \overline{u'^2}/k = 0.91$ ,  $\alpha_{22} = 0.91$ , and  $\alpha_{33} = 0.17$ . The corresponding ratio  $\sigma_w^2/(\sigma_u^2 + \sigma_v^2)$  is equal to 0.093. Values of the three closure constants unique to the Wilson et al. (1998) closure were unchanged from their recommendation.

## 4. Results

### a. The “host flow”

Figure 3 is a comparison of the friction velocity  $u_{*p}$  derived from the profiles of  $\bar{u}(z)$  and  $\bar{T}(z)$  on the tower, with ( $u_{*r} = \sqrt{-\overline{u'w'}}$ ) measured by the reference sonic anemometer at  $z/h = 2$  (after a rotation set  $\bar{v} = \bar{w} = 0$ ). Nothing in the analysis to follow depends on the agreement of these estimates of  $u_*$ ; their evident correlation makes it plausible to suggest, however, that above the modified boundary layer of our sparse array there was (as we had hoped) a relatively normal constant stress layer. Consistent with this suggestion is the fact (Figs. 4a,b) that standard deviations of the velocity fluctuations at  $z/h = 2$  were not too different from customary values in the atmospheric surface layer (Garratt 1978, 1992). No relationship with overall wind direction  $\bar{\theta}$  is evident. Figure 4c shows that within-canopy ratios  $\sigma_w^2/(\sigma_u^2 + \sigma_v^2)$  scatter without bias around the equilibrium value (0.093) inferred from the reference sonic anemometer, trending to smaller values with larger instability.

### b. Conditional sampling

As a first check on the measured time series, we “binned” velocity samples according to the instantaneous wind direction  $\beta$  relative to the symmetry axes of the array (for results shown, bin width was  $5^\circ$ ). Figure 5 shows a histogram of (reduced) wind direction, over 30 min, for each of two sonic anemometers at A locations ( $z/h = 1/2$ ) and the associated conditional mean values of cup wind speed and TKE, normalized on the

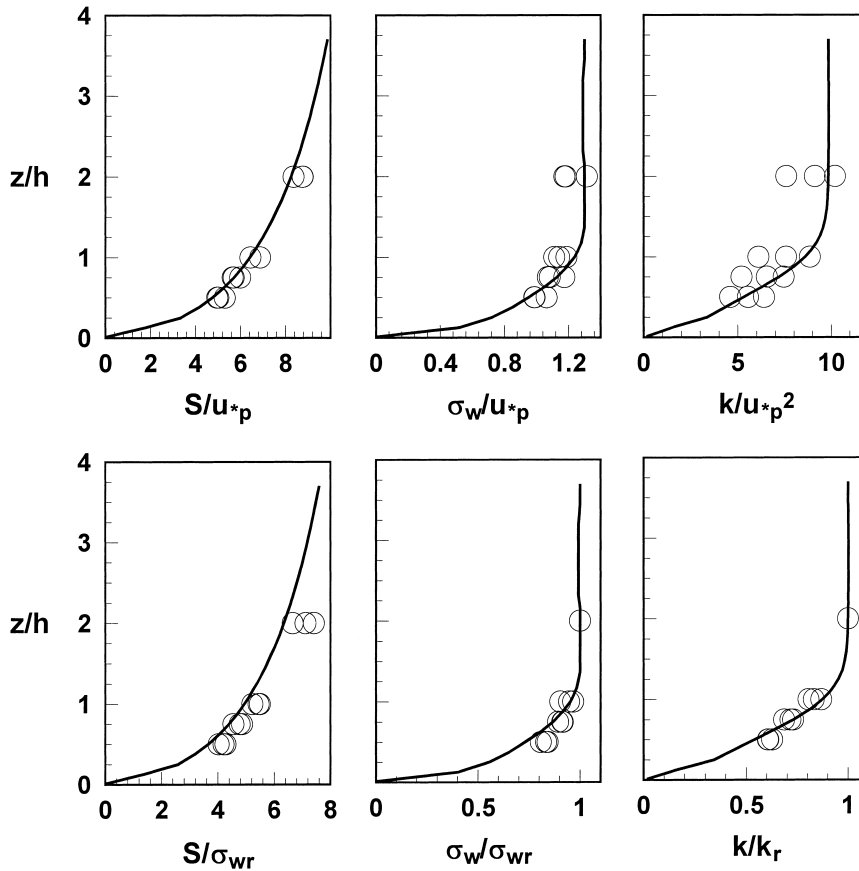


FIG. 8. Vertical profiles of cup wind speed  $S = \sqrt{u^2 + v^2}$ , of  $\sigma_w$  of the vertical velocity, and of  $k$  ( $\circ$ ) in the middle of the unit cell (position C) in comparison with results of the wind model (solid line).

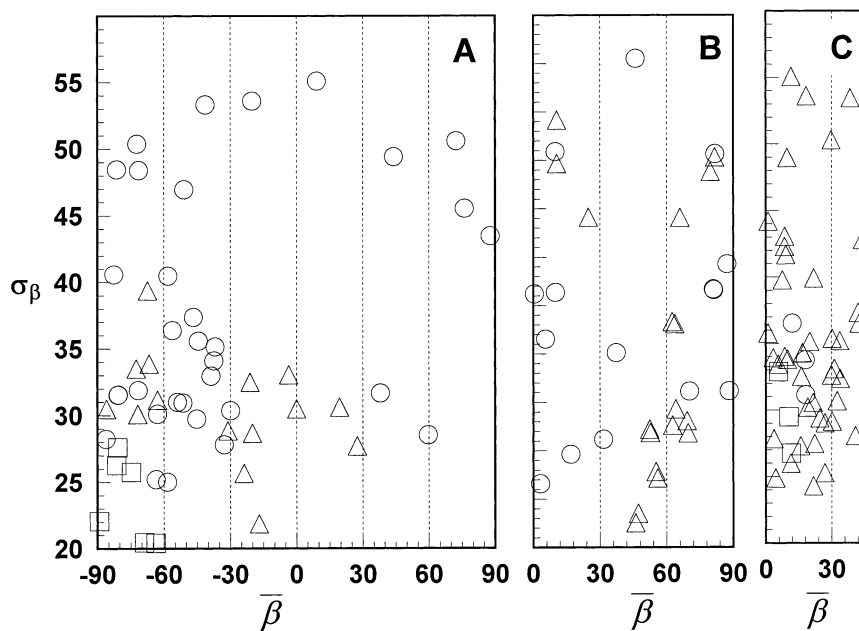


FIG. 9. Standard deviation of wind direction  $\sigma_\beta$  at heights  $z/h = 1/2$  ( $\circ$ ),  $3/4$  ( $\Delta$ ), and  $1$  ( $\square$ ) vs (reduced) mean wind direction  $\bar{\beta}$ .

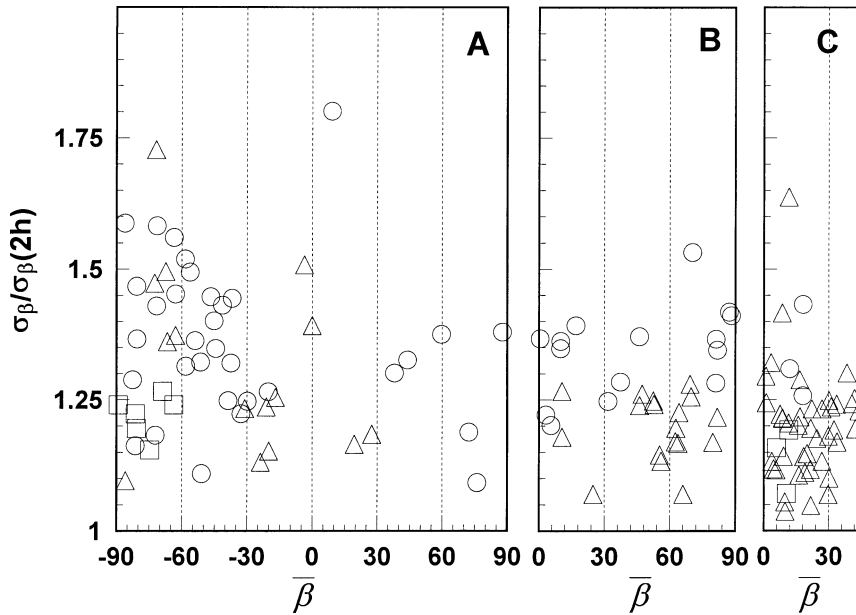


FIG. 10. Standard deviation of wind direction normalized on overhead value ( $\sigma_{\beta}/\sigma_{\beta r}$ ) at heights  $z/h = 1/2$  ( $\circ$ ),  $3/4$  ( $\triangle$ ), and  $1$  ( $\square$ ) vs (reduced) mean wind direction  $\bar{\beta}$ .

(respective) 30-min unconditional mean values. The two sonic anemometers were oriented differently with respect to the mean wind, and thus different regions of the range in reduced wind direction were sampled; one may not place much confidence in the conditionally sampled statistics at angles  $\beta$  for which  $t_i/T$  (the time fraction within a  $5^\circ$  bin centered at  $\beta$ ) is small. Symbols

indicate the angular locations of the most important blockages and corridors.

Angular regions of this diagram corresponding to high relative frequency of the approach angle permit an examination of the main symmetry effects of the distribution of drag nodes. In Fig. 5 at  $\beta = -90^\circ$  there is a minimum in conditional mean wind speed and TKE,

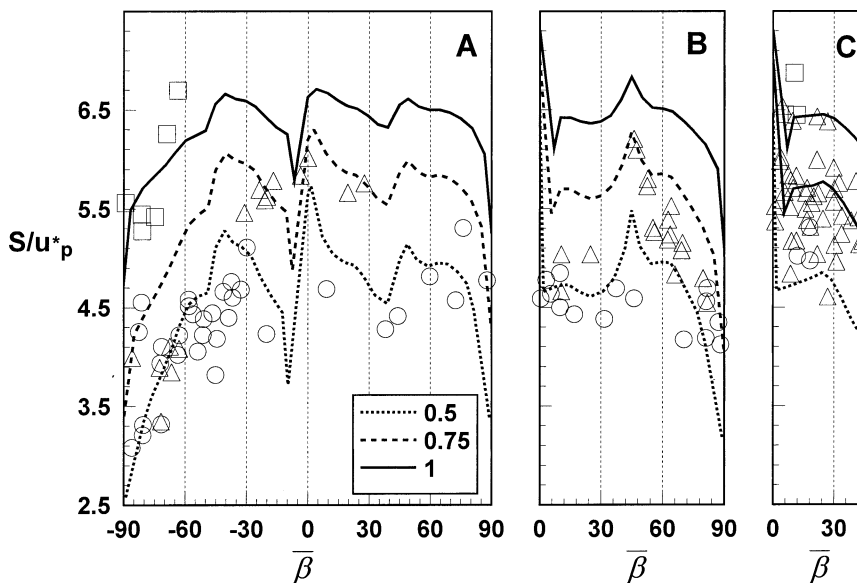


FIG. 11. Normalized cup wind speed  $S/u_{*p}$  at heights  $z/h = 1/2$  ( $\circ$ ),  $3/4$  ( $\triangle$ ), and  $1$  ( $\square$ ) vs local (reduced) mean wind direction  $\bar{\beta}$ , in comparison with results of the wind model (model's  $S/u_{*p}$  plotted at the predicted local  $\bar{\beta}$  for each location).

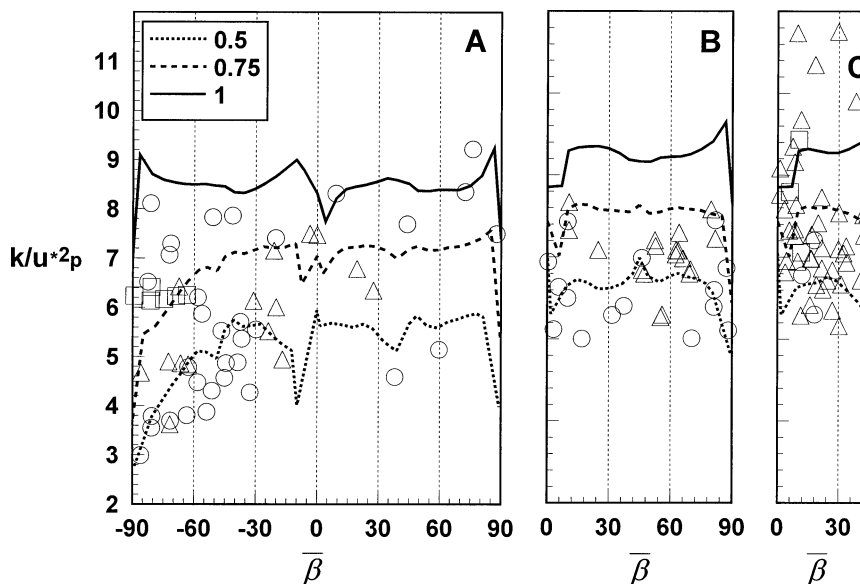


FIG. 12. Normalized TKE  $k/u_p^2$  at heights  $z/h = 1/2$  ( $\circ$ ),  $3/4$  ( $\Delta$ ), and  $1$  ( $\square$ ) vs local (reduced) mean wind direction  $\bar{\beta}$ , in comparison with results of the wind model.

with a symmetric recovery on either side (symmetry through  $\beta = -90^\circ$ ; the offset of this symmetry axis from precisely  $-90^\circ$  may indicate misalignment and misplacement of the anemometer with respect to the array, and the finite size of the clumps). When  $\beta = -90^\circ$ , location A is in the very near lee of a clump, and one may expect that the instrument (at this angle) lies within a “quiet zone,” though probably one more restricted in its extent than is found in the lee of a wind-break (Wilson 1987; McNaughton 1988). Around  $\beta = -50^\circ$  there are peaks in wind speed and TKE, presumably due to the fact that the wind approaches A down the corridor(s) at  $\beta = -63^\circ$  and  $\beta = -45^\circ$ . Then, as the approach angle nears the blockage at  $\beta = -14^\circ$ , speed and TKE fall off. The recovery (i.e., increase) in speed and TKE expected at A as  $\beta$  passes through  $-14^\circ$  and into the principal corridor at  $\beta = 0^\circ$  is definitely seen at  $S_2$  (i.e., right-hand figure) but is missing at  $S_1$ ; this is probably due to the fact that for sonic anemometer  $S_1$  during this run, angles near  $\beta = 0^\circ$  were on the tail of the histogram (one must also note there is a blockage to be considered at  $\beta = +20.6^\circ$ ). At positive  $\beta$ , the clearest feature is the blockage at  $\beta = +90^\circ$  (right-hand figure, i.e., sonic anemometer  $S_2$ ).

Figure 6 shows corresponding results from two instruments at B locations, placed at  $z/h = 3/4$ . Reflection symmetry is indicated fairly clearly about  $\beta = \pm 45^\circ$  (corridor angles), less clearly at  $\beta = \pm 90^\circ$ , and is hard to distinguish at all (though theoretically mandatory) at  $\beta = 0^\circ$ . For C locations (Fig. 7), symmetry is expected (and observed) about the corridor angle at  $\beta = 0^\circ$  and about the blockage angle at  $\beta = -45^\circ$  (the expected symmetry about  $\beta = +45^\circ$  is not evident, but this again

may be an artifact due to  $\beta = +45^\circ$  lying on the tail of the histogram of Fig. 7).

### c. Horizontal inhomogeneity of the flow

Figure 8 gives profiles at position C of cup wind speed  $S = \sqrt{u^2 + v^2}$ , standard deviation  $\sigma_w$  of the vertical velocity, and TKE  $k$  with the corresponding predictions of the numerical model. The good agreement between observed and modeled variables suggests that normalization of observations using properties from the reference sonic anemometer would have been acceptable. Both properties are attenuated with increasing depth below the top of the canopy, just as is observed in a regular plant canopy; the extinction coefficients are smaller than those typical of a uniform corn canopy, however. It would be convenient if wind statistics in a sparse canopy were represented adequately by those that would be seen on a tower placed at random in some convenient opening. However cup wind speeds  $S$  measured in the middle of the cell (i.e., at C) were *not* spatially representative, even for our exceptionally open canopy, for, depending on the wind direction, simultaneous measurements taken elsewhere in the canopy were substantially different (inhomogeneity in  $\sigma_w$  was less dramatic); for example, at  $z/h = 3/4$ , normalized wind speed  $S/\sigma_{wr}$  at A was reduced to only about 50% of its value at C, as  $\bar{\beta}$  approached  $-90^\circ$ . It follows that even in an *extremely* sparse canopy, horizontal heterogeneity is important, in the sense that profiles from some convenient central point can hardly be said to be “representative.”

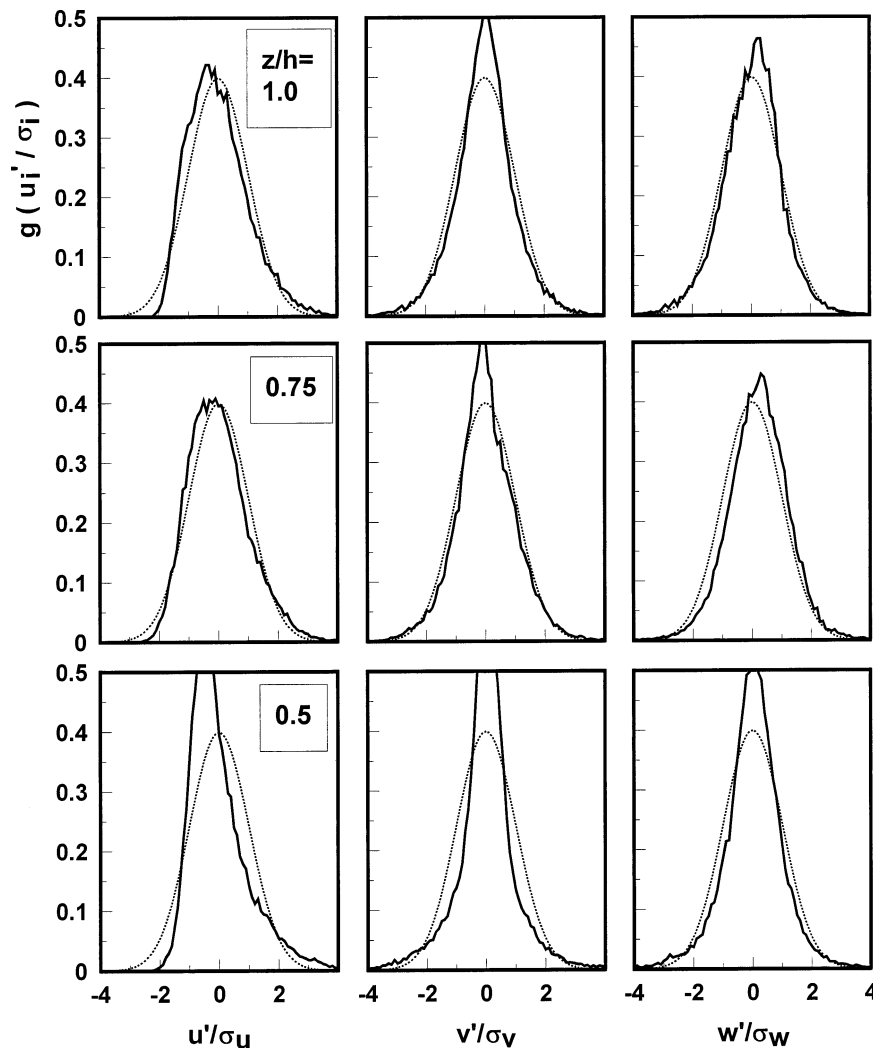


FIG. 13. Probability density functions  $g(\cdot)$  for the normalized velocity fluctuations ( $u'/\sigma_u$ , etc.) at  $z/h = (1/2, 3/4, 1)$  at location C. Dotted line shows a standardized normal distribution.

*d. Dependency of wind statistics on reduced wind angle, and comparison with numerical model*

Figure 9 gives observed values of the local standard deviation of wind direction  $\sigma_\beta$  at locations A, B, and C against the (local) mean (reduced) wind direction  $\bar{\beta}$ .<sup>1</sup> On Fig. 10, the local standard deviation of wind direction has been normalized by the corresponding value overhead at  $z/h = 2$ , from the reference sonic anemometer. It can be seen that  $\sigma_\beta(z)/\sigma_\beta(2h)$  is greater than 1 and that larger values are observed closer to ground. There is some suggestion from Fig. 9 that the variance in wind direction may be systematically reduced when the mean wind direction coincides with a corridor (this is very evident for the data from location B at  $z/h = 3/$

4). When variance in wind direction is normalized on the overhead value, however, this feature disappears, suggesting the pattern mentioned above on Fig. 9 is only due to insufficient sampling.

Figure 11 gives the observations of  $S/u_{*p}$  versus local mean reduced wind direction  $\bar{\beta}$ , with the corresponding predictions  $S/u_*$  of the numerical model. The model was run for overhead wind directions of  $0^\circ, 2^\circ, 5^\circ, 10^\circ, 15^\circ, \dots, 45^\circ$ . On Fig. 11 and others to follow, for comparison with observations at A, B, and C within the canopy, predictions of the model have been organized using the (predicted) local mean wind direction.

The variation with  $\bar{\beta}$  of the modeled variables at  $z = 2h$  (not shown on Fig. 11) was very weak, and suggests that normalization of observations using properties from the reference sonic anemometer would have been acceptable. At position A (for which, as we noted earlier, there is reflection symmetry of velocity statistics about

<sup>1</sup> We initially considered excluding from further analysis all runs with  $\sigma_\beta > 40^\circ$  but chose not to do so in case this procedure might illegitimately have biased our results.

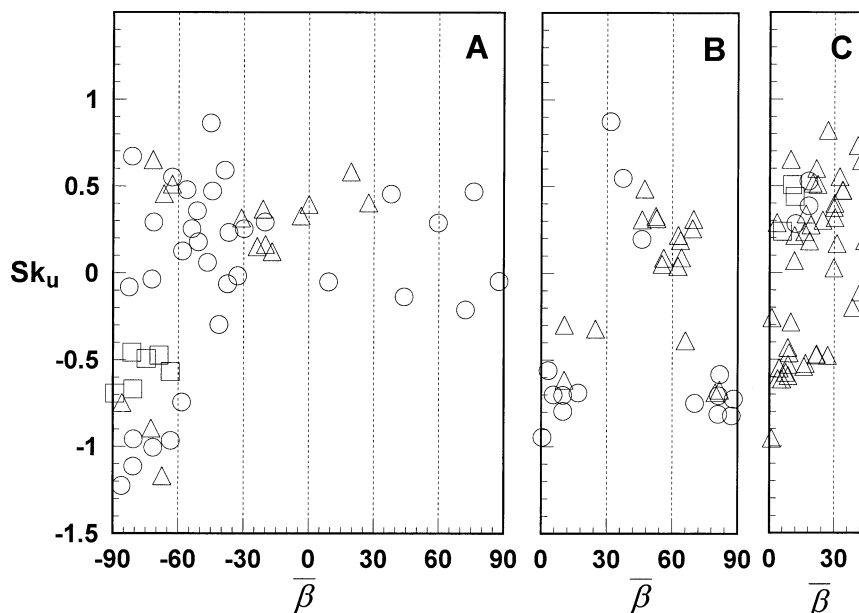


FIG. 14. Skewness  $Sk_u$  of the local alongwind velocity component at heights  $z/h = 1/2$  ( $\circ$ ),  $3/4$  ( $\Delta$ ), and  $1$  ( $\square$ ) vs local reduced mean wind direction  $\bar{\beta}$  for locations A, B, and C.

$\bar{\beta} = -90^\circ$  and about  $\bar{\beta} = +90^\circ$ ), just as in the earlier “conditionally sampled” statistics, we see in the mean angular dependence of the unconditional statistics the dominating influence of blockages by nearby clumps, most important at  $\bar{\beta} = -90^\circ, -14^\circ, +37^\circ$ , and  $+90^\circ$ , and of corridors at  $\bar{\beta} = 0^\circ$  and  $\pm 45^\circ$ .

At B the corridor angles are the same as at A, but the main blockage angle is  $27^\circ$ . Figure 11 shows that the normalized mean wind speed at B is larger when the wind is oriented along the corridors at  $0^\circ$  and  $45^\circ$  and is reduced in the blockages at  $27^\circ$  and  $90^\circ$ .

A numerical model of the type used here represents the fluctuations in overhead wind direction through the values of the velocity standard deviations  $\sigma_{u,v}$  specified at the top boundary. The exaggerated sharpness of the model variability around  $\bar{\beta} = 0^\circ$  caused us to wonder whether, in effect, model results do not sufficiently capture the “smearing” of observed statistics as the wind swings to and away from the corridors and blockages (i.e., exaggerated influence of the symmetries). Thus, we block-averaged model output in bins of width  $\pm 5^\circ$  about the central angles (not shown). Although this averaging somewhat reduced the amplitude of the swing through  $\bar{\beta} = 0^\circ$ , the effect overall was minimal.

Figure 12 shows the observed angular dependency of TKE at A, B, and C in comparison with corresponding results of the numerical model. Observed TKE data are more scattered relative to the model than were the wind speed data, and perhaps the best one can say of the model is that, at A anyway, it has (at least) captured the sole unambiguous feature of the observations: that when the mean (reduced) wind direction  $\bar{\beta} = -90^\circ$ , location A is a quiet zone, sheltered by the nearby up-

wind clump (but note that in these quiet zones, velocity skewness is high). When  $\bar{\beta} = +90^\circ$ , the sheltering clump is sufficiently far upwind (fetch to the clump is  $\frac{3}{4}d$ , i.e.,  $3.5h$ ) that “protection” is reduced.

#### e. Probability density functions, skewness, and kurtosis

Figure 13 gives simultaneous probability density functions (pdfs) of the normalized velocity fluctuations ( $u'/\sigma_u$ , etc.) measured at location C over 30 min (1620–1650 local time 11 September) at  $z/h = (0.5, 0.75, 1)$ . For each anemometer, prior to calculation of the pdfs, time series were rotated to ensure  $\bar{v} = 0$ , and standardized Gaussian distributions also have been plotted for comparison. The streamwise fluctuation  $u'$  is positively skewed,  $Sk_u > 0$ , close to ground, and the vertical fluctuation  $w'$  is negatively skewed. These are the characteristics normally seen in a plant canopy (Kaimal and Finnigan 1994, 80–81) and imply dominance of the turbulence by gusts. Figure 14 gives the observed skewness  $Sk_u$  of the alongwind component versus local reduced mean wind direction and confirms that locations that (for given  $\bar{\beta}$ ) lie in the near lee of a clump demonstrate more strongly negative  $Sk_u$  (especially evident at A for  $\bar{\beta}$  nearing  $-90^\circ$ ). Skewness at B presents an interesting pattern (though again, it may be a result of biased sampling), negative at either end of the range ( $0^\circ, 90^\circ$ ), that is, in both the channel ( $0^\circ$ ) and in the blockage ( $90^\circ$ , when a clump lies directly upwind in close proximity at distance  $d/2$ ), but positive in the corridor at  $45^\circ$ .

## 5. Conclusions

We have shown that a representation of the mean wind speed and TKE throughout a regular sparse canopy can be attained on the basis of observations from only a few points of measurement. Without any filtering of those observations, a complex but systematic pattern in mean wind speed emerges, reflecting the distribution of the drag nodes in a manner that is consistent with intuition and with the numerical model. By the criterion of our observations, the numerical model may be promising as an *interpolative* tool for the mean wind speed and direction. The TKE data are more widely scattered about the corresponding model results than are the mean wind data, but, assuming this to be a deficiency of the model, it does not unduly impact the calculation of the mean wind, which is affected by  $k$  through the eddy viscosity ( $K \propto k^{1/2}$ ).

Even though this is an extremely sparse canopy (LAI = 0.09), the inhomogeneity of the wind statistics is severe, and velocity pdfs are highly skewed in the near wakes of the clumps of plants, just as in a uniform canopy. Nevertheless, the partitioning ratios  $\sigma_w^2/k$  (etc.) of TKE into its components are not very different from their values in a normal surface layer.

Last, an aspect of this analysis worth mentioning is that the results of the very model we set out to “test” emerged as the factor encouraging us to believe what we were seeing (and discouraging us from the step of rejecting periods of record that scattered points across our otherwise orderly graphs).

*Acknowledgments.* Financial support of the Natural Sciences and Engineering Research Council of Canada (NSERC) is acknowledged. We thank Olivier Zurfluh of INRA for his help with the field work and subsequent analyses, and we thank many others of INRA whose help in planting the sparse canopy was very much appreciated.

## REFERENCES

- Dyer, A. J., 1974: A review of flux profile relationships. *Bound.-Layer Meteor.*, **7**, 363–372.
- Garratt, J. R., 1978: Transfer characteristics for a heterogeneous surface of large aerodynamic roughness. *Quart. J. Roy. Meteor. Soc.*, **104**, 491–502.
- , 1992: *The Atmospheric Boundary Layer*. Cambridge University Press, 316 pp.
- Kaimal, J. C., and J. J. Finnigan, 1994: *Atmospheric Boundary Layer Flows: Their Structure and Measurement*. Oxford University Press, 289 pp.
- McNaughton, K. G., 1988: Effects of windbreaks on microclimate. *Windbreak Technology*, J. R. Brandle, D. L. Hintz, and J. W. Sturrock, Eds., Elsevier Science, 17–40.
- Raupach, M. R., J. J. Finnigan, and Y. Brunet, 1996: Coherent eddies and turbulence in vegetation canopies. *Bound.-Layer Meteor.*, **78**, 351–382.
- Wilson, J. D., 1987: On the choice of a windbreak porosity profile. *Bound.-Layer Meteor.*, **38**, 37–49.
- , and T. K. Flesch, 1999: Wind and tree sway in forest cutblocks, III: A windflow model to diagnose spatial variation. *Agric. For. Meteor.*, **93**, 259–282.
- , J. J. Finnigan, and M. R. Raupach, 1998: A first-order closure for disturbed plant canopy flows, and its application to windflow through a canopy on a ridge. *Quart. J. Roy. Meteor. Soc.*, **124**, 705–732.